

Non-perturbative two-pion exchange contributions to the nucleon-nucleon interaction in covariant baryon chiral perturbation theory

Chun-Xuan Wang,¹ Jun-Xu Lu,^{2,1} Yang Xiao,³ and Li-Sheng Geng^{4,5,6,*}

¹*School of Physics, Beihang University, Beijing 102206, China*

²*School of Space and Environment, Beihang University, Beijing 102206, China*

³*School of Physics, Beihang University, Beijing 102206, China*

China & Université Paris-Saclay, CNRS/IN2P3, IJCLab, 91405 Orsay, France

⁴*School of Physics, Beihang University, Beijing 102206, China.*

⁵*Beijing Key Laboratory of Advanced Nuclear Materials and Physics, Beihang University, Beijing, 102206, China*

⁶*School of Physics and Microelectronics, Zhengzhou University, Zhengzhou, Henan 450001, China*

We calculate the non-perturbative two-pion exchange (TPE) contributions to the NN interaction in covariant baryon chiral perturbation theory. We study how the non-perturbative resummation affects the NN phase shifts for partial waves with $J \geq 3$ and $L \leq 6$. No significant differences are observed between the non-perturbative phase shifts and perturbative ones for most partial waves except for 3D_3 , for which the non-perturbative resummation greatly improves the description of the phase shifts. However, a significant cutoff dependence is found for this partial wave and a reasonable description of the phase shifts can only be obtained with a particular cutoff. Furthermore, we compare the so-obtained non-perturbative phase shifts with those obtained in the heavy baryon chiral perturbation theory. We show that the contributions from relativistic non-perturbative TPE are more moderate than those from the non-relativistic TPE obtained in the dimensional regularization scheme. A proper convergence pattern is observed for most of the partial waves studied except for 3F_3 , 3F_4 , and 3H_6 , for which the subleading TPE contributions are a bit strong. We find that for H and I partial waves, the OPE alone can already describe the phase shifts reasonably well.

PACS numbers: 21.30.-x

I. INTRODUCTION

Deriving the nucleon-nucleon (NN) interaction continues to be one of the most important topics in nuclear physics. Starting from the seminal idea of Yukawa [1] to describe the nuclear force in a field-theoretical manner, a number of high-precision phenomenological NN interactions have been constructed, such as Reid93 [2], Argonne V₁₈ [3], and CD-Bonn [4]. Although these interactions describe experiment data well, they are not directly linked to the underlying theory of the strong interaction, Quantum Chromodynamics (QCD). So far, the two most widely accepted model-independent approaches describing the NN interaction based on QCD are lattice QCD and chiral effective field theory (ChEFT). In the past decades, with the rapidly increasing computational resources and improvements in algorithms, lattice QCD simulations have been employed to derive the NN interaction from first principles [5–7] and remarkable progress has been made [8–10]. However, most lattice QCD simulations of the NN interaction still remain in the non-physical regime [11, 12]. On the other hand, chiral effective field theory has been successfully applied to study the NN interaction since the pioneering works of Weinberg [13, 14]. ChEFT is based on chiral symmetry of QCD and its spontaneous and explicit breakings. In ChEFT, the long range interaction is provided by the exchange of the Nambu-Goldstone bosons (pions in the u and d two flavor sector and the pseudoscalar nonet in the u , d , and s three flavor sector), and the short range interaction is described by the so-called low-energy constants (LECs) that encode the effects of degrees of freedom with energies larger than the chiral symmetry breaking scale, $\Lambda_{\chi SB}$. Nowadays, the chiral nuclear force has been constructed in the heavy-baryon scheme up to the fifth order [15–17] and becomes the de facto standard in ab initial nuclear structure and reaction studies [18–21].

Recently, a covariant power counting approach similar to the extended-on-mass-shell scheme in the one-baryon sector was proposed for the NN interaction [22, 23], with the full structure of the Dirac spinor retained. At leading order (LO), the covariant chiral nuclear force with five LECs can already provide a reasonably good description of the NN phase shifts for $J = 0$ and 1 partial waves [22]. In addition, the unique features of the 1S_0 partial wave, i.e., the pole position of the virtual bound state and the zero amplitude at the scattering momentum 340 MeV [24], can be well reproduced [25]. This framework has also been successfully applied to study lattice QCD NN interactions [26, 27],

*E-mail: lisheng.geng@buaa.edu.cn

hyperon-nucleon interactions [28–33], and $\Lambda_c N$ interaction [34, 35]. In Ref. [36], the renormalizability of the LO covariant chiral NN interaction was investigated in detail, which indeed shows some interesting improvements, e.g., in the puzzling 3P_0 channel.

Clearly, the LO covariant NN interaction still cannot reach the accuracy required for realistic applications, e.g., for many-body nuclear structure studies. To further improve the description of the NN phase shifts, higher order contributions need to be taken into account, which contain contact terms and two-pion exchanges. Up to NLO, there are 17 LECs in the covariant scheme [23], which contribute to all the partial waves with $J = 0, 1, 2$. At NNLO, no further LECs appear. In Ref. [37], the covariant TPE has been calculated perturbatively up to order $\mathcal{O}(p^3)$ for higher partial waves with $L \geq 2$. It was shown that the contributions of relativistic TPE are more moderate than those of the non-relativistic TPE at the perturbative level. Since the nucleon-nucleon system is non-perturbative in nature, it is necessary to explicitly check how the non-perturbative effect affects the TPE contributions in the covariant scheme, especially for the D and F partial waves, where the non-perturbative effects are expected to be relatively strong.¹

In this work, we start from the covariant chiral Lagrangians [38] and calculate the non-perturbative TPE up to order $\mathcal{O}(p^3)$. To resum the potential, we solve the Blankenbecler and Sugar (BbS) equation [39] in which the two intermediate nucleons are equally off-shell. Then, we calculate the phase shifts for higher partial waves of $J \geq 3$ and $L \leq 6$ and compare the resulting phase shifts with the perturbative ones of Ref. [37] and non-relativistic non-perturbative ones of Ref. [40].

This article is organized as follows. In Sec. II, we briefly revisit the power counting rule specified in Ref. [23] and spell out the covariant πN Lagrangians. In Sec. III, we explain how to construct the leading and subleading non-perturbative TPE, paying particular attention to the difference between the non-perturbative treatment with the perturbative treatment of Ref. [37]. The notations for the scattering equation and phase shifts are specified in Sec. IV. We show the partial wave phase shifts in Sec. V and discuss about the cutoff dependence and convergence, followed by a short summary and outlook in Sec. VI.

II. CHIRAL LAGRANGIAN

Following Ref. [37], the power counting rule applied in the present work is based on the naive dimensional analysis. For a certain Feynman diagram with L loops, the chiral dimension (n_χ) is computed as

$$\nu = 4L - 2N_\pi - N_n + \sum_k kV_k, \quad (1)$$

where N_π (N_n) refers to the number of internal pion (nucleon) propagators, and V_k is the number of k th-order vertices. According to the power counting rule of Eq. (1), for the purpose of including the contributions to the NN interaction from the pion exchanges up to NNLO, one needs to compute the Feynman diagrams shown in Figs. 1, 2, 3. The relevant Lagrangians for the πN vertices read [38]

$$\mathcal{L}_{\pi N}^{(1)} = \bar{\Psi} \left(i\not{D} - M + \frac{g_A}{2} \not{\psi} \gamma_5 \right) \Psi, \quad (2)$$

$$\mathcal{L}_{\pi N}^{(2)} = c_1 \langle \chi_+ \rangle \bar{\Psi} \Psi - \frac{c_2}{4M^2} \langle u^\mu u^\nu \rangle (\bar{\Psi} D_\mu D_\nu \Psi + h.c.) + \frac{c_3}{2} \langle u^2 \rangle \bar{\Psi} \Psi - \frac{c_4}{4} \bar{\Psi} \gamma^\mu \gamma^\nu [u_\mu, u_\nu] \Psi, \quad (3)$$

with the axial vector coupling $g_A = 1.29$ [19], the nucleon mass $M = 939$ MeV, the pion mass $m_\pi = 139$ MeV [41], the pion decay constant $f_\pi = 92.4$ MeV, and the low-energy constants $c_1 = -1.39$, $c_2 = 4.01$, $c_3 = -6.61$, $c_4 = 3.92$ [42] (all in units of GeV^{-1}). The SU(2) matrix $u = \exp\left(\frac{i\Phi}{2f_\pi}\right)$, the pion and nucleon fields Φ and Ψ read

$$\Phi = \begin{pmatrix} \pi^0 & \sqrt{2}\pi^+ \\ \sqrt{2}\pi^- & -\pi^0 \end{pmatrix}, \quad \Psi = \begin{pmatrix} p \\ n \end{pmatrix}, \quad (4)$$

¹ In the present work, we refrain from studying the lower partial waves with $J = 0, 1, 2$, because they involve unknown LECs up to NNLO and therefore a dedicate fitting to data is needed for a meaningful study.

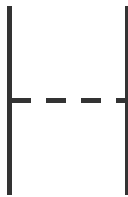


FIG. 1: One-pion exchange diagram at LO ($O(p^0)$). The pion-nucleon vertices refer to vertices from $\mathcal{L}_{\pi N}^{(1)}$

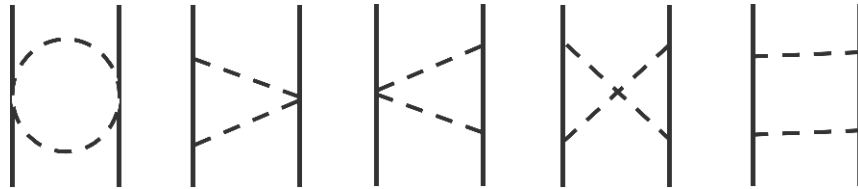


FIG. 2: Two-pion exchange diagrams at NLO ($O(p^2)$). The pion-nucleon vertices refer to vertices from $\mathcal{L}_{\pi N}^{(1)}$

and $\chi_+ = u^\dagger \chi u + u \chi u^\dagger$ with $\chi = \mathcal{M} = \text{diag}(m_\pi^2, m_\pi^2)$. The covariant derivative is defined as

$$D_\mu = \partial_\mu + \Gamma_\mu, \quad (5)$$

$$\Gamma_\mu = \frac{1}{2} (u^\dagger \partial_\mu u + u \partial_\mu u^\dagger), \quad (6)$$

$$u_\mu = i (u^\dagger \partial_\mu u - u \partial_\mu u^\dagger). \quad (7)$$

From the above Lagrangians, we can obtain the products of isospin and coupling factors for the TPE diagrams shown in Figs. 1, 2, 3. For details, we refer to Table. I of Ref. [37].

III. TWO-PION EXCHANGE CONTRIBUTIONS

We calculate the two-pion exchanges in the center-of-mass (C.M.) frame and in the isospin limit $m_u = m_d$. Because the large non-zero baryon mass at the chiral limit leads to the so-called power counting breaking (PCB) problem, one should recover the power counting rule defined in Eq. (1). Here, we adopt the extended-on-mass-shell (EOMS) scheme and extend it to the two-baryon sector to remove the PCB terms, which has been well established in the one-baryon [43–45] and meson-baryon sectors [42, 46]. We use FeynCalc [47–49] to decompose the full TPE potential into the scalar integrals A0, B0, C0, and D0 multiplied with certain polynomials and fermion bilinears, and then calculate the potential numerically with the help of OneLoop [50, 51].

Different from Ref. [37], we focus in the present work on the off-shell TPE contributions which are necessary for the non-perturbative treatment. For an off-shell nucleon $u(p, M)$ with momentum $p = (p^0, \vec{p})$, the equation of motion $\not{p}u(p, M) = Mu(p, M)$ is no longer applicable. Instead, one now has

$$\not{p}u(p, M) = \begin{pmatrix} p^0 - E + M & 0 \\ 0 & E - p^0 + M \end{pmatrix} u(p, M), \quad (8)$$

where $E = \sqrt{|\vec{p}|^2 + M^2}$ is the energy of the nucleon. For on-shell nucleons, one has $p^0 = E$ and then the normal equation of motion is recovered.

Next, we evaluate the various classes of Feynman diagrams one by one. In writing down the potential, the explicit expressions of the potential will not be given due to their complexity ².

² They could be obtained as a Mathematica notebook from the authors upon request

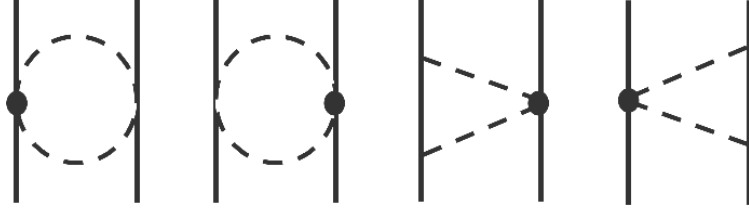


FIG. 3: Two-pion exchange diagrams at NNLO ($O(p^3)$). The black dots denote vertices from $\mathcal{L}_{\pi N}^{(2)}$

A. Leading order ($O(p^0)$) results

At LO, we only have the one-pion exchange (OPE) diagram shown in Fig. 1. The OPE potential can be expressed as

$$V_{\text{OPE}} = \frac{g_A^2}{4f_\pi^2} \frac{\bar{u}(p_3)\gamma^\mu\gamma_5(p_{1\mu} - p_{3\mu})u(p_1)\bar{u}_4(p_4)\gamma^\nu\gamma_5(p_{4\nu} - p_{2\nu})u(p_2)}{(p_3 - p_1)^2 + m_\pi^2}, \quad (9)$$

which does not contain power counting breaking terms.

B. Next-to-leading order ($O(p^2)$) results

At NLO, there are five TPE diagrams as shown in Fig. 2, which from left to right correspond to the football diagram, the two triangle diagrams, the crossed box diagram, and the planar box diagram, respectively. The corresponding TPE potentials at this order can be written as

$$V_{\text{Box}} = \frac{-ig_A^4}{16f_\pi^4} \int \frac{d^4l}{(2\pi)^4} \frac{\bar{u}(p_3)\gamma^\nu\gamma_5(l_\nu + p_{3\nu} - p_{1\nu})(\not{p}_1 - \not{l} + M)\gamma^\mu\gamma_5\not{l}_\mu u(p_1)\bar{u}(p_4)\gamma^\tau\gamma_5(l_\tau + p_{2\tau} - p_{4\tau})}{((p_2 + l)^2 + M^2)((p_1 - l)^2 + M^2)} \times \frac{(\not{p}_2 + \not{l} + M)\gamma^\rho\gamma_5\not{l}_\rho u(p_2)}{(l^2 + m_\pi^2)((l + p_2 - p_4)^2 + m_\pi^2)}, \quad (10)$$

$$V_{\text{Cross}} = \frac{-ig_A^4}{16f_\pi^4} \int \frac{d^4l}{(2\pi)^4} \frac{\bar{u}(p_3)\gamma^\nu\gamma_5(l_\nu + p_{3\nu} - p_{1\nu})(\not{p}_1 - \not{l} + M)\gamma^\mu\gamma_5\not{l}_\mu u(p_1)\bar{u}(p_4)\gamma^\tau\gamma_5\not{l}_\tau(\not{p}_4 - \not{l} + M)}{((p_1 - l)^2 + M^2)((p_4 - l)^2 + M^2)} \times \frac{\gamma^\rho\gamma_5(\not{l}_\rho + p_{2\rho} - p_{4\rho})u(p_2)}{(l^2 + m_\pi^2)((l + p_2 - p_4)^2 + m_\pi^2)}, \quad (11)$$

$$V_{\text{Football}} = \frac{1}{2} \frac{-i}{16f_\pi^4} \int \frac{d^4l}{(2\pi)^4} \frac{\bar{u}(p_3)\gamma^\mu(2\not{l}_\mu + p_{1\mu} - p_{3\mu})u(p_1)\bar{p}_4\gamma^\nu(2\not{l}_\nu + p_{4\nu} - p_{2\nu})u(p_2)}{(l^2 + m_\pi^2)((l + p_4 - p_2)^2 + m_\pi^2)}, \quad (12)$$

$$V_{\text{TriangleL}} = \frac{-ig_A^2}{16f_\pi^4} \int \frac{d^4l}{(2\pi)^4} \frac{\bar{u}(p_3)\gamma^\mu(2\not{l}_\mu + p_{4\mu} - p_{2\mu})u(p_1)\bar{u}(p_4)\gamma^\nu\gamma_5(l_\nu + p_{4\nu} - p_{2\nu})(\not{p}_2 - \not{l} + M)\gamma^\rho\gamma_5(-\not{l}_\rho)u(p_2)}{((p_2 - l)^2 + M^2)(l^2 + m_\pi^2)((l + p_4 - p_2)^2 + m_\pi^2)}, \quad (13)$$

$$V_{\text{TriangleR}} = \frac{-ig_A^2}{16f_\pi^4} \int \frac{d^4l}{(2\pi)^4} \frac{\bar{u}(p_3)\gamma^\nu\gamma_5(l_\nu + p_{3\nu} - p_{1\nu})(\not{p}_1 - \not{l} + M)\gamma^\rho\gamma_5(-\not{l}_\rho)u(p_1)\bar{u}(p_4)\gamma^\mu(2\not{l}_\mu + p_{3\mu} - p_{1\mu})u(p_2)}{((p_1 - l)^2 + M^2)(l^2 + m_\pi^2)((l + p_3 - p_1)^2 + m_\pi^2)}. \quad (14)$$

The corresponding PCB terms at NLO in helicity basis are

$$V_{\text{Football}}^{\text{PCB}} = 0, \quad (15)$$

$$V_{\text{TriangleL}}^{\text{PCB}} = 4H_1 M^2 \ln\left(\frac{\mu}{M}\right), \quad (16)$$

$$V_{\text{TriangleR}}^{\text{PCB}} = 4H_1 M^2 \ln\left(\frac{\mu}{M}\right), \quad (17)$$

$$V_{\text{Cross}}^{\text{PCB}} = -4H_1 M^2 \left[3 \ln\left(\frac{\mu}{M}\right) - 1 \right], \quad (18)$$

$$V_{\text{Box}}^{\text{PCB}} = -4H_1 M^2 \left[\ln\left(\frac{\mu}{M}\right) + 1 \right], \quad (19)$$

where μ refers to the renormalization scale and is set at 1 GeV in our numerical study. H_1 is the inner product of the initial and final helicity basis and reads

$$H_1 = \left[|\bar{\lambda}_1 + \lambda_1| \cos\left(\frac{\theta}{2}\right) + |\bar{\lambda}_1 - \lambda_1| \sin\left(\frac{\theta}{2}\right) \right] \left[|\bar{\lambda}_2 + \lambda_2| \cos\left(\frac{\theta}{2}\right) - |\bar{\lambda}_2 - \lambda_2| \sin\left(\frac{\theta}{2}\right) \right], \quad (20)$$

where $\lambda_{1,2}, \bar{\lambda}_{1,2}$ denote the helicities of incoming and outgoing particles, respectively, and θ is the scattering angle.

C. Next-to-next-to-leading order ($\mathcal{O}(p^3)$) results

At NNLO, we have four diagrams as shown in Fig. 3. In general, we only need to replace one of the πN vertices at $\mathcal{O}(p)$ in the diagrams of Fig. 2 with the corresponding $\mathcal{O}(p^2)$ vertex. Note that no box diagram and crossed box diagram appears at this order because there is no πNN vertex at $\mathcal{O}(p^2)$. Corresponding to the four terms c_1, c_2, c_3, c_4 in the $\mathcal{O}(p^2)$ πN vertices, the potential of the football (left) diagram in which the left πN vertex is replaced reads

$$V_{\text{FootballL}}^{c_1} = \frac{1}{2} \frac{-im_\pi^2}{16f_\pi^4} \int \frac{d^4 l}{(2\pi)^4} \frac{\bar{u}(p_3)u(p_1)\bar{u}(p_4)\gamma^\mu(2l_\mu + p_{4\mu} - p_{2\mu})u(p_2)}{(l^2 + m_\pi^2)((l + p_1 - p_3)^2 + m_\pi^2)}, \quad (21)$$

$$V_{\text{FootballL}}^{c_2} = \frac{1}{8M^2} \frac{-i}{16f_\pi^4} \int \frac{d^4 l}{(2\pi)^4} \frac{\bar{u}(p_3)(l \cdot p_1(l \cdot p_1 + p_1 \cdot p_1 - p_3 \cdot p_1) + l \cdot p_3(l \cdot p_3 + p_1 \cdot p_3 - p_3 \cdot p_3))u(p_1)}{(l^2 + m_\pi^2)((l + p_1 - p_3)^2 + m_\pi^2)} \\ \times \bar{u}(p_4)\gamma^\mu(2l_\mu + p_{4\mu} - p_{2\mu})u(p_2), \quad (22)$$

$$V_{\text{FootballL}}^{c_3} = \frac{1}{2} \frac{-i}{16f_\pi^4} \int \frac{d^4 l}{(2\pi)^4} \frac{\bar{u}(p_3)(l \cdot l + l \cdot p_1 - l \cdot p_3)u(p_1)\bar{u}(p_4)\gamma^\mu(2l_\mu + p_{4\mu} - p_{2\mu})u(p_2)}{(l^2 + m_\pi^2)((l + p_1 - p_3)^2 + m_\pi^2)}, \quad (23)$$

$$V_{\text{FootballL}}^{c_4} = \frac{1}{2} \frac{-i}{16f_\pi^4} \int \frac{d^4 l}{(2\pi)^4} \frac{\bar{u}(p_3)(-\gamma^\mu(l_\mu + p_{1\mu} - p_{3\mu})\gamma^\nu l_\nu + \gamma^\mu l_\mu \gamma^\nu(l_\nu + p_{1\nu} - p_{3\nu}))u(p_1)}{(l^2 + m_\pi^2)((l + p_1 - p_3)^2 + m_\pi^2)} \\ \times \bar{u}(p_4)\gamma^\mu(2l_\mu + p_{4\mu} - p_{2\mu})u(p_2), \quad (24)$$

and the whole football (left) potential can be expressed as

$$V_{\text{FootballL}} = c_1 \times V_{\text{FootballL}}^{c_1} + c_2 \times V_{\text{FootballL}}^{c_2} + c_3 \times V_{\text{FootballL}}^{c_3} + c_4 \times V_{\text{FootballL}}^{c_4}. \quad (25)$$

Similarly, the potential of the triangle (left) diagram reads,

$$V_{\text{TriangleL}} = c_1 \times V_{\text{TriangleL}}^{c_1} + c_2 \times V_{\text{TriangleL}}^{c_2} + c_3 \times V_{\text{TriangleL}}^{c_3} + c_4 \times V_{\text{TriangleL}}^{c_4}, \quad (26)$$

where

$$V_{\text{TriangleL}}^{c_1} = \frac{1}{2} \frac{-im_\pi^2 g_A^2}{16f_\pi^4} \int \frac{d^4 l}{(2\pi)^4} \frac{\bar{u}(p_3)u(p_1)\bar{u}(p_4)\gamma^\rho\gamma_5(l_\rho + p_{4\rho} - p_{2\rho})(\not{p}_2 - \not{l} + M)\gamma^\tau\gamma_5(-l_\tau)u(p_2)}{(l^2 + m_\pi^2)((l + p_1 - p_3)^2 + m_\pi^2)((p_2 - l)^2 + M^2)}, \quad (27)$$

$$V_{\text{TriangleL}}^{c_2} = \frac{1}{8M^2} \frac{-ig_A^2}{16f_\pi^4} \int \frac{d^4 l}{(2\pi)^4} \frac{\bar{u}(p_3)(l \cdot p_1(l \cdot p_1 + p_1 \cdot p_1 - p_3 \cdot p_1) + l \cdot p_3(l \cdot p_3 + p_1 \cdot p_3 - p_3 \cdot p_3))u(p_1)}{(l^2 + m_\pi^2)((l + p_1 - p_3)^2 + m_\pi^2)((p_2 - l)^2 + M^2)} \times u(p_4)\gamma^\rho\gamma_5(l_\rho + p_{4\rho} - p_{2\rho})(\not{p}_2 - \not{l} + M)\gamma^\tau\gamma_5(-l_\tau)u(p_2), \quad (28)$$

$$V_{\text{TriangleL}}^{c_3} = \frac{1}{2} \frac{-ig_A^2}{16f_\pi^4} \int \frac{d^4 l}{(2\pi)^4} \frac{\bar{u}(p_3)(l \cdot l + l \cdot p_1 - l \cdot p_3)u(p_1)\bar{u}(p_4)\gamma^\rho\gamma_5(l_\rho + p_{4\rho} - p_{2\rho})(\not{p}_2 - \not{l} + M)\gamma^\tau\gamma_5(-l_\tau)u(p_2)}{(l^2 + m_\pi^2)((l + p_1 - p_3)^2 + m_\pi^2)((p_2 - l)^2 + M^2)}, \quad (29)$$

$$V_{\text{TriangleL}}^{c_4} = \frac{1}{2} \frac{-ig_A^2}{16f_\pi^4} \int \frac{d^4 l}{(2\pi)^4} \frac{\bar{u}(p_3)(-\gamma^\mu(l_\mu + p_{1\mu} - p_{3\mu})\gamma^\nu l_\nu + \gamma^\mu l_\mu \gamma^\nu(l_\nu + p_{1\nu} - p_{3\nu}))u(p_1)}{(l^2 + m_\pi^2)((l + p_1 - p_3)^2 + m_\pi^2)((p_2 - l)^2 + M^2)} \times u(p_4)\gamma^\rho\gamma_5(l_\rho + p_{4\rho} - p_{2\rho})(\not{p}_2 - \not{l} + M)\gamma^\tau\gamma_5(-l_\tau)u(p_2). \quad (30)$$

The potential for the football (right) diagram and triangle (right) diagrams can then be obtained via simple exchanges of $p_1 \leftrightarrow p_2$ and $p_3 \leftrightarrow p_4$. The PCB terms at this order in helicity basis read,

$$V_{\text{FootballL}}^{\text{PCB}} = 0, \quad (31)$$

$$V_{\text{FootballR}}^{\text{PCB}} = 0, \quad (32)$$

$$V_{\text{TrigL}}^{\text{PCB}} = 6c_1 H_1 M m_\pi^2 \left[2 \ln \left(\frac{\mu}{M} \right) + 1 \right] + \dots, \quad (33)$$

$$V_{\text{TrigR}}^{\text{PCB}} = 6c_1 H_1 M m_\pi^2 \left[2 \ln \left(\frac{\mu}{M} \right) + 1 \right] + \dots. \quad (34)$$

In deriving the potential, to be consistent, we must adopt the same approximation as that of the BbS equation, i.e., the two nucleons are equally off the mass shell [39, 52]. In this approximation, the incoming momenta in the center-of mass frame are expressed as $p_1 = (\sqrt{s}/2, \mathbf{p})$ and $p_2 = (\sqrt{s}/2, -\mathbf{p})$, the outgoing momenta as $p_3 = (\sqrt{s}/2, \mathbf{p}')$ and $p_4 = (\sqrt{s}/2, -\mathbf{p}')$, and the transferred momentum as $q = (0, \mathbf{p}' - \mathbf{p})$.

D. Iterated OPE

To avoid double counting the OPE contribution in the non-perturbative treatment of TPE contributions, one needs to subtract the contribution of iterated OPE (IOPE) which appears in the box diagram in the case of on-shell intermediate nucleons. We calculate the IOPE contribution numerically, i.e.,

$$V_{\text{IOPE}}(p', p|\sqrt{s}) = \int \frac{k^2 dk}{(2\pi)^3} V_{\text{OPE}}(p', k|\sqrt{s}) G_{\text{BbS}}(k|\sqrt{s}) V_{\text{OPE}}(k, p|\sqrt{s}), \quad (35)$$

where $p = |\mathbf{p}|$, $p' = |\mathbf{p}'|$, \sqrt{s} is the total energy of the two-nucleon system in the C.M. frame, V_{OPE} is the OPE potential in the LSJ representation and G_{BbS} is the propagator adopted in the BbS equation. The integral above suffers from the same ultraviolet divergence as the scattering equation and thus needs to be properly regularized. We introduce an exponential regulator function f^Λ as

$$f^\Lambda(k) = \exp[-(k/\Lambda)^{2n}] \quad (36)$$

and choose $n = 3$ following Ref. [53]. In this way, the OPE potential V_{OPE} in Eq. (35) should be substituted with

$$\begin{aligned} V_{\text{OPE}}(p', k|\sqrt{s}) &\rightarrow f^\Lambda(k) V_{\text{OPE}}(p', k|\sqrt{s}), \\ V_{\text{OPE}}(k, p|\sqrt{s}) &\rightarrow f^\Lambda(k) V_{\text{OPE}}(k, p|\sqrt{s}). \end{aligned} \quad (37)$$

IV. SCATTERING EQUATION

To calculate the non-perturbative contributions of TPE, one has to resum the above potential up to infinite order. In principle, one should solve the Bethe-Salpeter(BS) equation [54] which reads schematically in operator form

$$T = W + WGT \quad (38)$$

where T is the scattering amplitude, W is the sum of all irreducible diagrams, and G is the relativistic four dimensional two-nucleon propagator. However, the solution of such a four dimensional integral equation is quite difficult and one often turns to its three-dimensional reduction. The BS equation can be divided into two coupled equations,

$$T = W + WgT, \quad (39)$$

$$W = \tilde{V} + \tilde{V}(G - g)W, \quad (40)$$

where g is the three-dimensional propagator, which will be specified below, and in this way, Eq. (39) is a three dimensional equation. Up to NNLO, Eq. (40) simplifies to

$$W \approx \tilde{V} + V_{\text{OPE}}(G - g)V_{\text{OPE}}, \quad (41)$$

where the potential takes the following form

$$W = V_{\text{CON}}^{\text{LO}} + V_{\text{CON}}^{\text{NLO}} + V_{\text{OPE}} + V_{\text{TPE}}^{\text{NLO}} + V_{\text{TPE}}^{\text{NNLO}} - V_{\text{IOPE}}, \quad (42)$$

in which the first two terms refer to the contact terms at LO ($\mathcal{O}(p^0)$) and NLO ($\mathcal{O}(p^2)$), while the next three terms denote the contributions from OPE and TPE at NLO and NNLO. The last term represents the iterated OPE contribution, i.e., $V^{\text{OPE}} \cdot g \cdot V^{\text{OPE}}$.

For the relativistic three-dimensional propagator g , we choose the one proposed by Blankenbecler and Sugar [39] (BbS) which has the practical advantage that the potential becomes energy-independent [55]. The BbS equation projected into the LSJ representation in operator form reads

$$T_{l'l}^{sj}(p', p|\sqrt{s}) = V_{l'l}^{sj}(p', p|\sqrt{s}) + \sum_{l''} \int \frac{k^2 dk}{(2\pi)^3} V_{l'l''}^{sj}(p', k|\sqrt{s}) \frac{M^2}{E_k} \frac{1}{p^2 - k^2 + i\epsilon} T_{l''l}^{sj}(k, p|\sqrt{s}). \quad (43)$$

The iteration of V in the BbS equation requires cutting V off for high momenta to avoid ultraviolet divergence. This is achieved in the following way:

$$V_{l'l}^{sj}(p', p|\sqrt{s}) = f_R(p)V(p', p|\sqrt{s})f_R(p'), \quad (44)$$

where the regulator function is chosen as,

$$f_R(p) = f_R^{\text{sharp}}(p) = \theta(\Lambda^2 - p^2). \quad (45)$$

It should be stressed that we use the same cutoff in the scattering equation as the one in the IOPE contribution. In fact, the phase shifts are basically unchanged if we only vary the cutoff in the IOPE piece but fix the cutoff in the scattering equation since it is known that the IOPE contributes little to scattering amplitudes for most partial waves [56].

The partial wave S matrix is related to the on-shell T matrix by

$$S_{l'l}^{sj}(p_{cm}) = \delta_{l'l}^{sj} + 2\pi i \rho T_{l'l}^{sj}(p_{cm}), \quad \rho = -\frac{|p_{cm}|M^2}{16\pi^2 E_{cm}} \quad (46)$$

where p_{cm} is the C.M. three momentum of the two-nucleon system. The phase space factor can be determined by the elastic unitarity of the BbS equation.

Phase shifts in the single channel case can be obtained from the S matrix via

$$S_{jj}^{0j} = \exp^{2i\delta_j^{0j}}, \quad S_{jj}^{1j} = \exp^{2i\delta_j^{1j}}. \quad (47)$$

To calculate the phase shifts in coupled channels, we adopt the Stapp parametrization [57] of the S matrix, which

can be written as

$$S = \begin{pmatrix} S_{--}^{1j} & S_{-+}^{1j} \\ S_{+-}^{1j} & S_{++}^{1j} \end{pmatrix} \quad (48)$$

$$= \begin{pmatrix} \exp^{i\delta_-^{1j}} & 0 \\ 0 & \exp^{i\delta_+^{1j}} \end{pmatrix} \begin{pmatrix} \cos(2\varepsilon) & i\sin(2\varepsilon) \\ i\sin(2\varepsilon) & \cos(2\varepsilon) \end{pmatrix} \begin{pmatrix} \exp^{i\delta_-^{1j}} & 0 \\ 0 & \exp^{i\delta_+^{1j}} \end{pmatrix} \quad (49)$$

$$= \begin{pmatrix} \cos(2\varepsilon)\exp^{2i\delta_-^{1j}} & i\sin(2\varepsilon)\exp^{i\delta_-^{1j}+i\delta_+^{1j}} \\ i\sin(2\varepsilon)\exp^{i\delta_-^{1j}+i\delta_+^{1j}} & \cos(2\varepsilon)\exp^{2i\delta_+^{1j}} \end{pmatrix} \quad (50)$$

where the subscript “+” refers to $j + 1$ and “-” to $j - 1$.

V. RESULTS AND DISCUSSIONS

In this section, the LO, NLO, and NNLO relativistic non-perturbative phase shifts with $J \geq 3$ and $L \leq 6$ are presented and compared with those of the perturbative counterparts [37], the non-relativistic counterparts obtained in the dimensional regularization (DR) scheme [40], the non-relativistic counterparts obtained with the spectral function regularization (SFR) scheme [58, 59], and the Nijmegen partial wave phase shifts [60]. For simplification, we use “NNLO-Per”, “NNLO-NR-DR”, “NNLO-NR-SFR” and “PWA93” to denote these results respectively in the following.

In the present work we concentrate on the partial waves to which up to NNLO contact terms do not contribute. Therefore, the cutoff is the only free parameter. Following the treatment of Ref. [40], we vary the cutoff between 600 and 1000 MeV in the present work and find that the best description of the phases shifts is obtained with a cutoff around 900 MeV. The fact that the cutoff used for NNLO studies is relatively larger than the usual value for LO or NLO studies has been noticed in the non-relativistic schemes [40], where it was pointed out that the large contribution of subleading TPE shifts the cutoff to a larger value. In the non-relativistic potential obtained in the DR scheme [40], a sharp cutoff with $\Lambda = 875$ MeV is used in solving the scattering equation, while for the non-relativistic results obtained with the SFR scheme [59] a local regulator function in coordinate space with $R = 1$ fm is used in solving the scattering equation³. In the following, we plot the phase shifts for each partial wave obtained with solely OPE and TPE contributions up to $T_{\text{lab}} = 280$ MeV where the first inelastic channel opens.

A. D wave

In D -wave, only 3D_3 is free of contact contributions up to NNLO in our covariant framework. The phase shifts are shown in Fig. 4. The NNLO non-perturbative phase shifts are in good agreement with PWA93 up to $T_{\text{lab}} = 250$ MeV, while the perturbative results keep increasing rapidly in the whole energy region. This indicates that the non-perturbative effect plays a crucial role for this partial wave. Similar conclusions have been drawn in Refs. [37, 61]. Compared with the NNLO-NR-DR scheme [40], we find that both the non-relativistic and our relativistic results can describe the phase shifts quite well below $T_{\text{lab}} = 100$ MeV. However, above 100 MeV, the relativistic correction is of visible size and helps to improve the description of phase shifts⁴. Compared with the LO and NLO results for this partial wave, the NNLO results describe the phase shifts significantly better. However, we notice that the differences between the NNLO and NLO results are much larger than those between the NLO and LO results. This indicates a quite large contribution from the subleading TPE, which implies that the convergence of our covariant nuclear force is questionable up to NNLO. Actually this is not surprising since the non-relativistic studies also suffer from such an extremely large subleading TPE contribution [40]. The spectral function regularization (SFR) method was proposed in Ref. [58] to deal with this problem by introducing a cutoff for the chiral loops. In our covariant framework based on the EOMS scheme, such a cutoff method is not practical. Higher order contributions may also be helpful to balance the large subleading TPE contribution as was shown in Ref. [62, 63]. This should be explicitly checked in the future.

It should be noted that for 3D_3 the phase shifts are sensitive to the choice of the cutoff, which is shown in Fig. 9. Varying the cutoff from 800 MeV to 1000 MeV, the phase shifts at $T_{\text{lab}} = 280$ MeV changes approximately from 10

³ With $R = 1$ fm one obtains the smallest $\bar{\chi}^2$ for all $J \geq 3$ and $L \leq 6$ partial waves among the choices of $R = 0.8, 0.9, 1.0, 1.1, 1.2$ fm

⁴ Note that the non-relativistic result for the 3D_3 partial wave is also dependent on the cutoff. The cutoff of 875 MeV is the optimum value for all the partial waves. A better description of the 3D_3 channel is possible if one fine-tunes the cutoff.

degree to -5 degree. This comes from the strong cutoff dependence of subleading TPE. Higher order contact terms may be of great help to weaken the cutoff dependence, as was done in Ref. [40] where the strong cutoff dependence of the NNLO-NR-DR results for the 1D_2 partial wave is significantly reduced once the contact terms of N³LO were introduced.

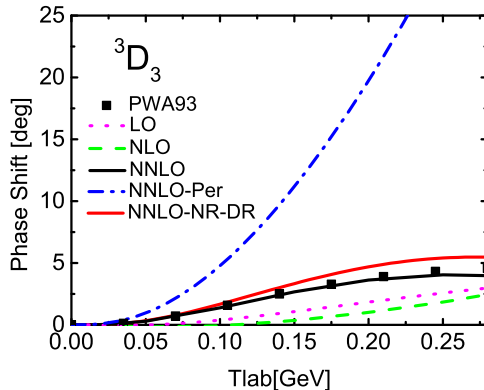


FIG. 4: 3D_3 phase shifts as a function of T_{lab} . The black dots denotes the PWA93 results [60]. The magenta dotted, green dashed, and black solid lines represent the relativistic non-perturbative LO, NLO, and NNLO phase shifts, respectively. For comparison we also show the non-relativistic counterparts (NNLO-NR-DR, red solid line) [40] and relativistic perturbative results at NNLO [37] (NNLO-Per, blue dash dotted line).

B. F wave

The F -wave phase shifts and mixing angle ϵ_3 are depicted in Fig. 5. We do not show the phase shifts of 3F_2 because in our covariant scheme, this partial wave involves NLO contact terms. In general, the non-perturbative phase shifts for all the F -waves are compatible with the perturbative results. For the 1F_3 , 3F_3 and 3F_4 partial waves, the non-perturbative phase shifts are slightly worse than the perturbative results while the non-perturbative treatment slightly improve the description of ϵ_3 . This indicates that for F -waves, the non-perturbative effect play an insignificant role. Compared with the non-relativistic results, both our covariant NNLO results and NNLO-NR-DR results could describe the PWA93 data with $T_{\text{lab}} \leq 100$ MeV equally well. However, in the higher energy region, the relativistic results are better, especially for the 3F_3 and 3F_4 partial waves. The relativistic correction plays a positive and non-negligible role for these two partial waves. On the other hand, the larger differences between the NNLO and NLO results (than those between the NLO and LO results) indicate that these two partial waves receive large subleading TPE contributions originated from the c_3 and c_4 terms.⁵ The mixing angle ϵ_3 is well described up to $T_{\text{lab}} = 250$ MeV in all the calculations. Both the higher order contributions and relativistic corrections do not have a visible effect on this mixing angle. Actually the OPE contribution alone can already describe the mixing angle well.

The F -wave phase shifts and mixing angle ϵ_3 obtained with different cutoffs are plotted in Fig. 9. We can see that the results with cutoff=800,900,1000 MeV are almost overlapping with each other, which implies a quite weak cutoff dependence.

C. G wave and higher partial waves

The G -, H -, and I -wave phase shifts and corresponding mixing angles ϵ_4 , ϵ_5 , and ϵ_6 are depicted in Fig. 6, 7, 8, respectively. For partial waves with $L \geq 4$, almost all the NNLO results can describe the PWA93 phase shifts up

⁵ For the 3F_3 and 3F_4 partial waves, the NNLO non-relativistic non-perturbative results obtained with the spectral function regularization (SPR) scheme [59] describe better the data, because the SFR scheme suppresses the strong short-range contribution from subleading TPE [58]. However, the SFR scheme worsens the description of some other channels, such as 3G_5 .

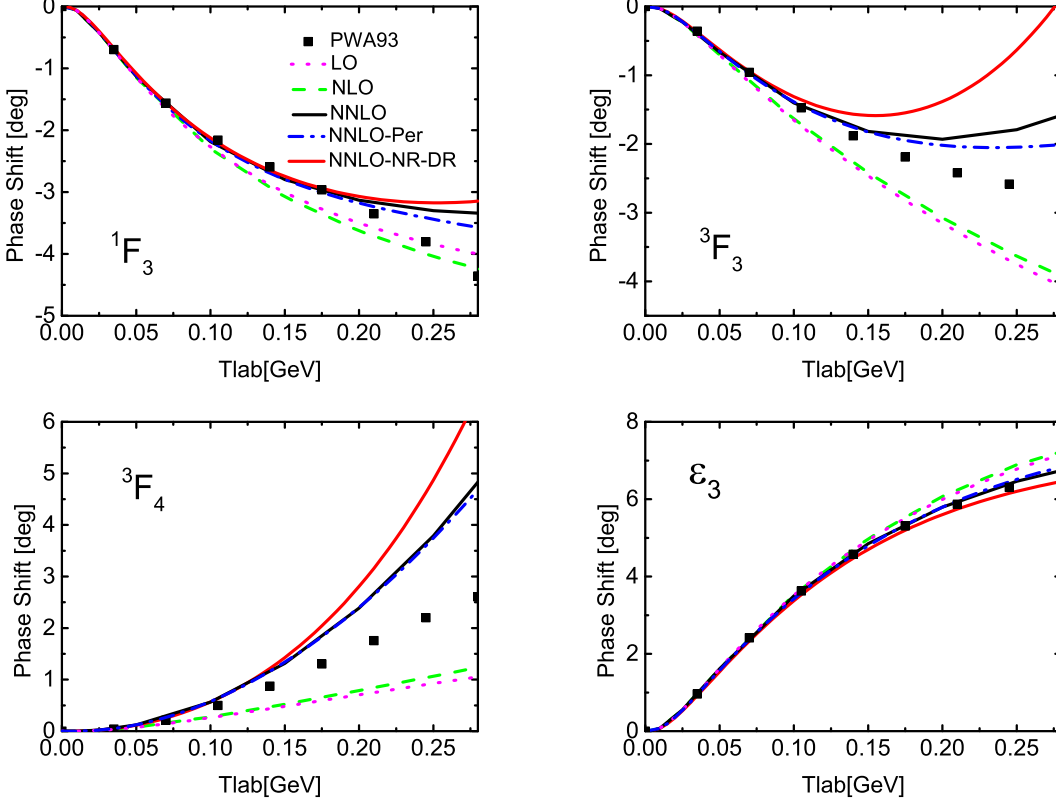


FIG. 5: Same as Fig. 4, but for the F -wave phase shifts and mixing angle ε_3 .

to $T_{\text{lab}} = 200$ MeV equally well. This indicates that neither the non-perturbative effect nor the relativistic effect contribute significantly at NNLO.

For the ${}^3G_3, {}^1G_4, {}^3G_4$ partial waves, the relativistic non-perturbative results are slightly worse than the perturbative results while they are better for 3G_5 . Compared with the non-relativistic results, the relativistic NNLO phase shifts are slightly better for ${}^3G_3, {}^1G_4, {}^3G_5$, while for 3G_4 and ε_4 , the two results almost overlap. For ${}^3G_3, {}^3G_4, \varepsilon_4$, the OPE alone does already a fairly good job, while for ${}^1G_4, {}^3G_5$, we find a visibly improved description from LO to NNLO indicating that the subleading TPE is still important for these two partial waves.

For the H -wave, the perturbative and non-perturbative ${}^1H_5, {}^3H_5$ phase shifts and mixing angle ε_5 are indistinguishable. The perturbative results are slightly better for 3H_4 while the non-perturbative results are slightly better for 3H_6 . For the ${}^3H_4, {}^1H_5, {}^3H_5$ partial waves, the relativistic results are slightly better than the non-relativistic results. For ε_5 , the phase shifts from different potentials are all very close to the PWA93 results up to $T_{\text{lab}} = 280$ MeV. Only for 3H_6 , the contribution of the subleading TPE seems to be a bit large for $T_{\text{lab}} \geq 150$ MeV. The behavior of the partial waves is quite similar to that of 3F_4 to which also a strong subleading TPE contributes.

The I -waves are almost in the same situation as the H -waves. The non-perturbative phase shifts are nearly identical to the perturbative phase shifts and nonrelativistic phase shifts, all of which are in good agreement with the PWA93 data. For 1I_6 , the TPE contribution slightly worsens the description while for 1I_7 it slightly improves the description. For all the H - and I -wave phase shifts, the OPE potential alone can describe the data reasonably well, which confirm the expectation that for higher partial waves, the TPE contribution is insignificant.

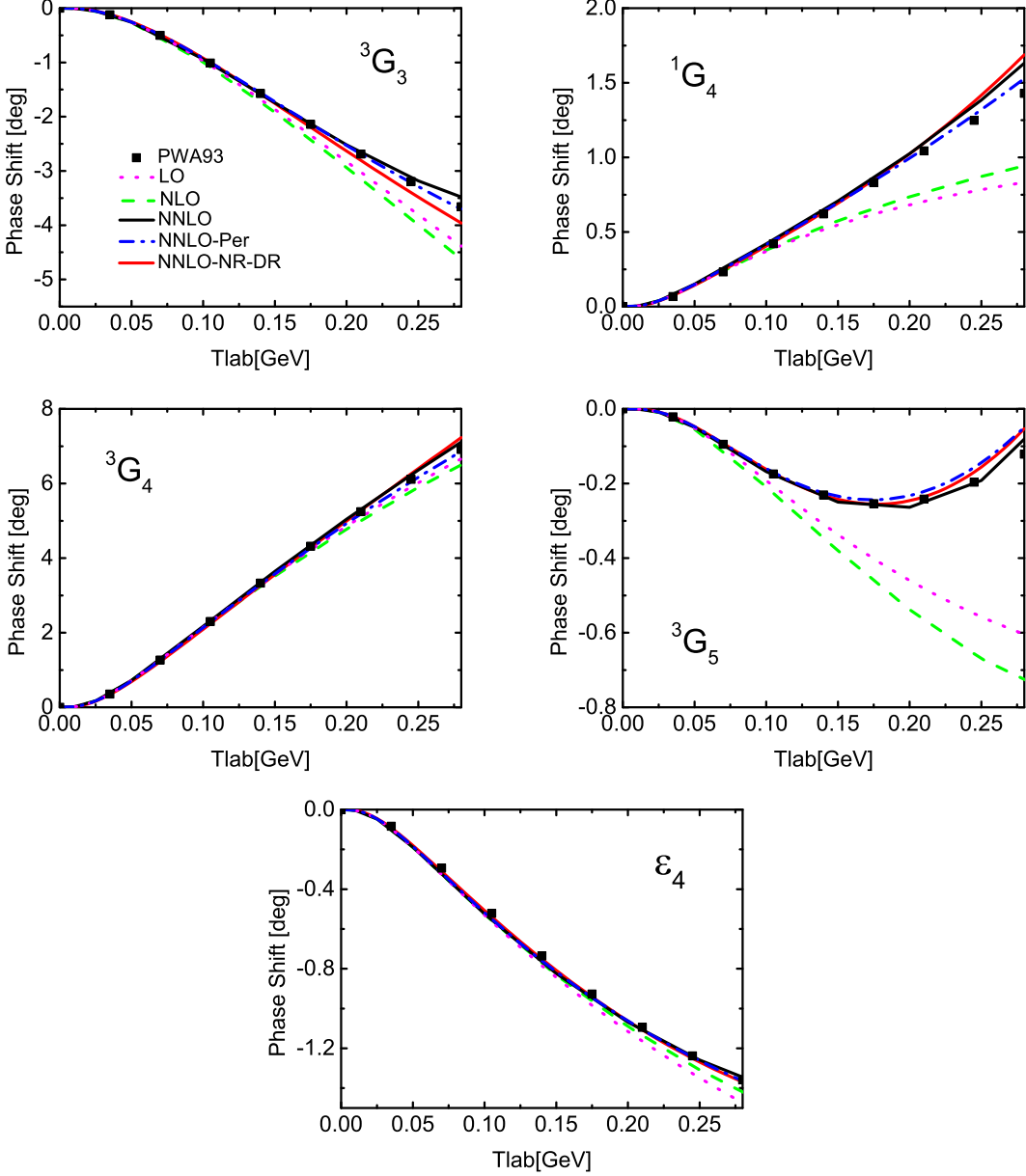


FIG. 6: Same as Fig. 4, but for the G -wave phase shifts and mixing angle ϵ_4 .

D. Quantitative comparisons

For the purpose of a more quantitative comparison of different theoretical results, in this subsection, we calculate the chisquare-like function $\tilde{\chi}^2$ defined as

$$\tilde{\chi}^2 = \sum_{i=1}^9 (\delta(i) - \delta_{\text{PWA}}(i))^2 \quad (51)$$

at $T_{\text{lab}}(i) = \{1, 5, 10, 25, 50, 100, 150, 200, 250\}$ MeV for the LO, NLO, NNLO relativistic non-perturbative TPE as well as the NNLO-Per and NNLO-NR-DR results, which are given in Table I in which $\tilde{\chi}_D^2$ only includes the contribution from 3D_3 , $\tilde{\chi}_F^2$ includes those from 1F_3 , 3F_3 , 3F_4 and ϵ_3 , $\tilde{\chi}_G^2$ contains the contributions from all the G -waves and mixing angle ϵ_4 , $\tilde{\chi}_H^2$, and $\tilde{\chi}_I^2$ are the same as for the G -waves. Compared with the relativistic perturbative results, the

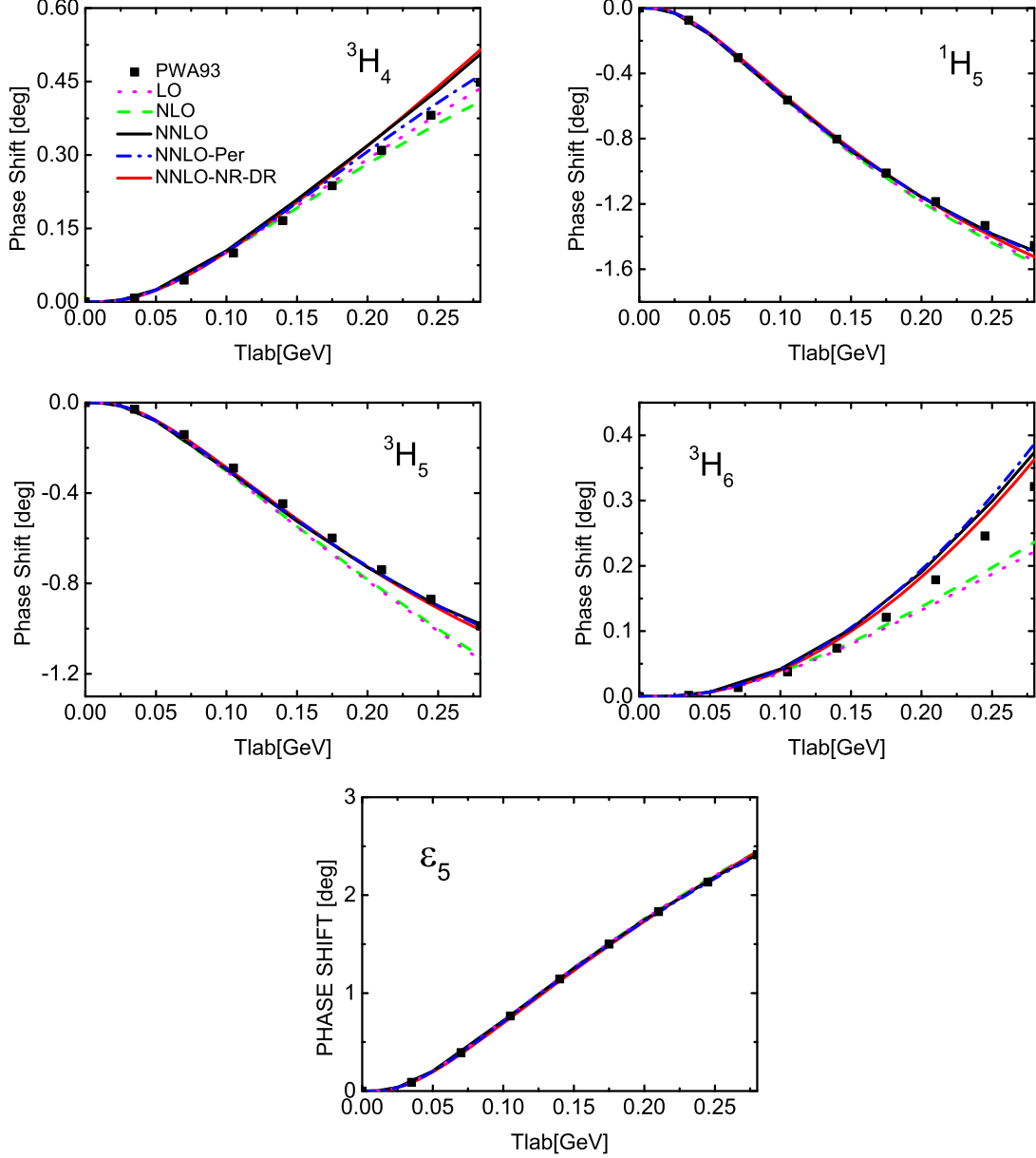


FIG. 7: Same as Fig. 4, but for the H -wave phase shifts and mixing angle ϵ_5 .

relativistic non-perturbative results have a much smaller $\tilde{\chi}_D^2$ at NNLO but slightly larger $\tilde{\chi}_F^2$ and $\tilde{\chi}_G^2$. Compared with the non-relativistic results, our covariant NNLO results lead to a much smaller $\tilde{\chi}^2$ for D -wave, F -waves, and G -waves. For higher partial waves, since the non-perturbative effect and the relativistic effect do not make much difference, $\tilde{\chi}_H^2$ and $\tilde{\chi}_I^2$ are almost the same for the covariant NNLO, NNLO-Per, and NNLO-NR-DR results. Furthermore, $\tilde{\chi}_H^2$ and $\tilde{\chi}_I^2$ at LO are relatively small and are already comparable with those at NNLO, which indicate the OPE contributions alone can describe the phase shifts well enough.

VI. SUMMARY AND OUTLOOK

Based on the covariant power counting rule proposed in Ref. [22, 23], we calculated the relativistic TPE potential up to NNLO ($O(p^3)$) and obtained the non-perturbative scattering amplitude by solving the BbS equation with the so-obtained potential. With this T matrix, we further calculated the chiral NN phase shifts for $J \geq 3$ and $L \leq 6$ to

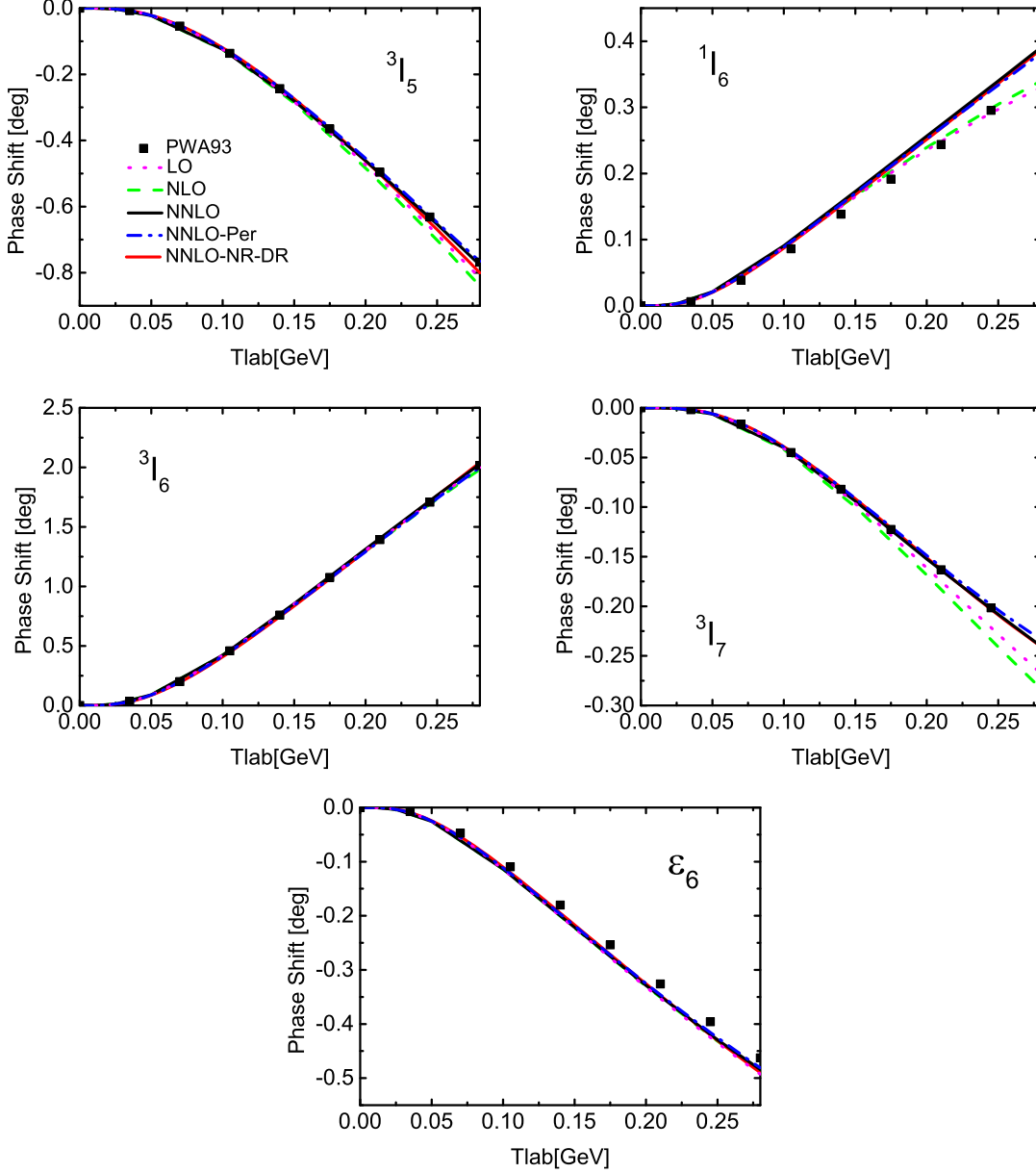


FIG. 8: Same as Fig. 4, but for the I -wave phase shifts and mixing angle ϵ_6 .

which no contact term contributes up to NNLO and then compared our results with the corresponding perturbative results and the non-relativistic results. We found that the non-perturbative effect is significant for the 3D_3 partial wave but insignificant for other higher partial waves we studied. Furthermore, a remarkable cutoff dependence is observed for this partial wave which can be cured by higher order contact interactions. We confirmed that the contributions of relativistic TPE are more moderate than their non-relativistic counterparts at the non-perturbative level. Moreover, we found that for most partial waves, the TPE contributions play a positive role in improving the descriptions but for the 3F_3 , 3F_4 and 3H_6 partial waves, the contribution from subleading TPE is a bit strong such that the resulting phase shifts become larger than the data. The non-relativistic results suffer from the same problem when the dimensional regularization method was applied to treat the ultraviolet divergence of chiral loops [40]. The abnormally large contribution of subleading TPE indicates that up to NNLO, the convergence is somehow questionable for these partial waves.

It should be stressed that the relativistic corrections for the $J \geq 3$ and $L \leq 6$ partial waves are indeed found to improve the description of the NN phase shifts as expected. Furthermore, although the non-perturbative effects play

TABLE I: $\tilde{\chi}^2$ defined in Eq. (51) for all $J \geq 3$ and $L \leq 6$ partial waves.

	LO	NLO	NNLO	NNLO-Per	NNLO-NR-DR
$\tilde{\chi}_D^2$	10.9	22.2	0.0129	10.1	2.38
$\tilde{\chi}_F^2$	5.65	5.03	4.28	3.73	14.0
$\tilde{\chi}_G^2$	1.03	1.48	0.0461	0.0144	0.117
$\tilde{\chi}_H^2$	0.0421	0.0420	0.0114	0.0116	0.0116
$\tilde{\chi}_I^2$	0.00458	0.00750	0.00476	0.00449	0.00416

a minor role for most higher partial waves we studied, we expect that they will play a more important role for lower partial waves of $J \leq 2$, as found in, e.g., Ref. [22]. In addition, the non-perturbative TPE contributions obtained in the present work set foundation for the construction of a high precision covariant chiral NN interaction. All of these will be left for future studies

VII. ACKNOWLEDGEMENTS

This work is supported in part by the National Natural Science Foundation of China under Grants No.11735003, No.11975041, and No.11961141004. Jun-Xu Lu is supported in part by the National Natural Science Foundation of China under Grants No.1210050991.

VIII. APPENDIX

In Fig. 9 we collect the phase shifts for all the partial waves obtained with different cutoffs varying from 800 MeV to 1000 MeV. We can see that for all the partial waves except 3D_3 , the results are quite stable and almost cutoff independent.

-
- [1] H. Yukawa, Proc. Phys. Math. Soc. Jap. **17**, 48 (1935).
 - [2] V. G. J. Stoks, R. A. M. Klomp, C. P. F. Terheggen, and J. J. de Swart, Phys. Rev. C **49**, 2950 (1994), nucl-th/9406039.
 - [3] R. B. Wiringa, V. G. J. Stoks, and R. Schiavilla, Phys. Rev. C **51**, 38 (1995), nucl-th/9408016.
 - [4] R. Machleidt, Phys. Rev. C **63**, 024001 (2001), nucl-th/0006014.
 - [5] N. Ishii, S. Aoki, and T. Hatsuda, Phys. Rev. Lett. **99**, 022001 (2007), nucl-th/0611096.
 - [6] S. Aoki, T. Hatsuda, and N. Ishii, Prog. Theor. Phys. **123**, 89 (2010), 0909.5585.
 - [7] S. R. Beane, W. Detmold, K. Orginos, and M. J. Savage, Prog. Part. Nucl. Phys. **66**, 1 (2011), 1004.2935.
 - [8] N. Barnea, L. Contessi, D. Gazit, F. Pederiva, and U. van Kolck, Phys. Rev. Lett. **114**, 052501 (2015), 1311.4966.
 - [9] C. Drischler, W. Haxton, K. McElvain, E. Mereghetti, A. Nicholson, P. Vranas, and A. Walker-Loud, Prog. Part. Nucl. Phys. **121**, 103888 (2021), 1910.07961.
 - [10] S. Aoki and T. Doi, Front. in Phys. **8**, 307 (2020), 2003.10730.
 - [11] M. Illa et al. (NPLQCD), Phys. Rev. D **103**, 054508 (2021), 2009.12357.
 - [12] C. McIlroy, C. Barbieri, T. Inoue, T. Doi, and T. Hatsuda, Phys. Rev. C **97**, 021303 (2018), 1701.02607.
 - [13] S. Weinberg, Phys. Lett. B **251**, 288 (1990).
 - [14] S. Weinberg, Nucl. Phys. B **363**, 3 (1991).
 - [15] E. Epelbaum, H. Krebs, and U. G. Meißner, Phys. Rev. Lett. **115**, 122301 (2015), 1412.4623.
 - [16] P. Reinert, H. Krebs, and E. Epelbaum, Eur. Phys. J. A **54**, 86 (2018), 1711.08821.
 - [17] D. R. Entem, R. Machleidt, and Y. Nosyk, Phys. Rev. C **96**, 024004 (2017), 1703.05454.
 - [18] E. Epelbaum, H.-W. Hammer, and U.-G. Meißner, Rev. Mod. Phys. **81**, 1773 (2009), 0811.1338.
 - [19] R. Machleidt and D. R. Entem, Phys. Rept. **503**, 1 (2011), 1105.2919.
 - [20] H. W. Hammer, S. König, and U. van Kolck, Rev. Mod. Phys. **92**, 025004 (2020), 1906.12122.

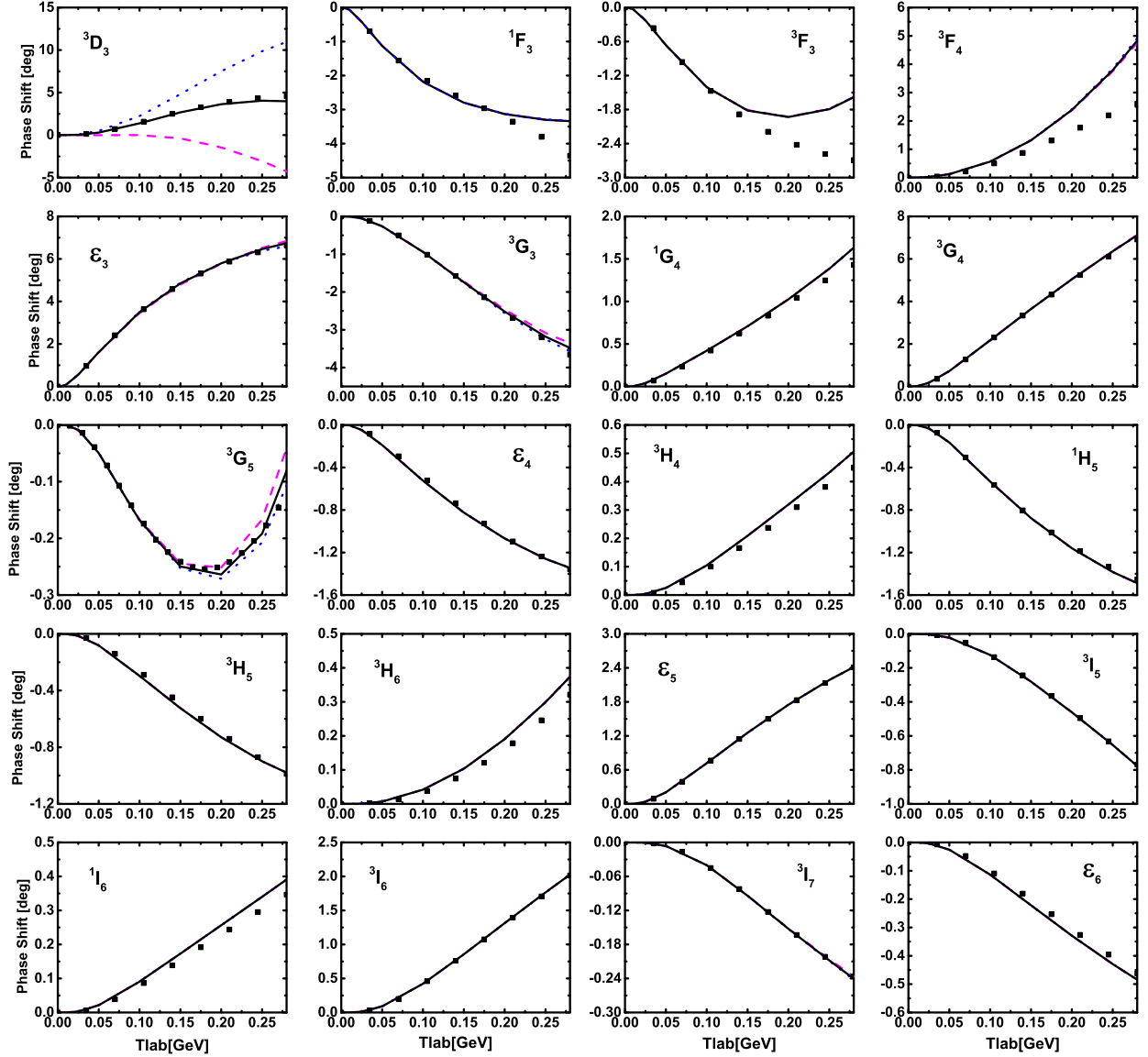


FIG. 9: Cutoff dependence of the covariant OPE and TPE results up to NNLO for $J \geq 3$ and $L \leq 6$ partial waves. The black dots denote the Nijmegen partial wave phase shifts [60]. The NNLO relativistic results obtained with cutoff = 800, 900, 1000 MeV are depicted with the blue dotted lines, the black solid lines, and the magenta dashed lines, respectively.

- [21] I. Tews, Z. Davoudi, A. Ekström, J. D. Holt, and J. E. Lynn, *J. Phys. G* **47**, 103001 (2020), 2001.03334.
- [22] X.-L. Ren, K.-W. Li, L.-S. Geng, B.-W. Long, P. Ring, and J. Meng, *Chin. Phys. C* **42**, 014103 (2018), 1611.08475.
- [23] Y. Xiao, L.-S. Geng, and X.-L. Ren, *Phys. Rev. C* **99**, 024004 (2019), 1812.03005.
- [24] M. Sánchez Sánchez, C. J. Yang, B. Long, and U. van Kolck, *Phys. Rev. C* **97**, 024001 (2018), 1704.08524.
- [25] X.-L. Ren, C.-X. Wang, K.-W. Li, L.-S. Geng, and J. Meng, *Chin. Phys. Lett.* **38**, 062101 (2021), 1712.10083.
- [26] Q.-Q. Bai, C.-X. Wang, Y. Xiao, and L.-S. Geng, *Phys. Lett. B*, 135745 (2020), 2007.01638.
- [27] Q.-Q. Bai, C.-X. Wang, Y. Xiao, and L.-S. Geng (2021), 2105.06113.
- [28] K.-W. Li, X.-L. Ren, L.-S. Geng, and B. Long, *Phys. Rev. D* **94**, 014029 (2016), 1603.07802.
- [29] K.-W. Li, X.-L. Ren, L.-S. Geng, and B.-W. Long, *Chin. Phys. C* **42**, 014105 (2018), 1612.08482.
- [30] K.-W. Li, T. Hyodo, and L.-S. Geng, *Phys. Rev. C* **98**, 065203 (2018), 1809.03199.
- [31] J. Song, K.-W. Li, and L.-S. Geng, *Phys. Rev. C* **97**, 065201 (2018), 1802.04433.
- [32] Z.-W. Liu, J. Song, K.-W. Li, and L.-S. Geng, *Phys. Rev. C* **103**, 025201 (2021), 2011.05510.
- [33] J. Song, Z.-W. Liu, K.-W. Li, and L.-S. Geng (2021), 2107.04742.
- [34] J. Song, Y. Xiao, Z.-W. Liu, C.-X. Wang, K.-W. Li, and L.-S. Geng, *Phys. Rev. C* **102**, 065208 (2020), 2010.06916.

- [35] J. Song, Y. Xiao, Z.-W. Liu, K.-W. Li, and L.-S. Geng (2021), 2104.02380.
- [36] C.-X. Wang, L.-S. Geng, and B. Long, *Chin. Phys. C* **45**, 054101 (2021), 2001.08483.
- [37] Y. Xiao, C.-X. Wang, J.-X. Lu, and L.-S. Geng, *Phys. Rev. C* **102**, 054001 (2020), 2007.13675.
- [38] N. Fettes, U.-G. Meissner, M. Mojzis, and S. Steininger, *Annals Phys.* **288**, 273 (2000), [Erratum: *Annals Phys.* 288, 249–250 (2001)], hep-ph/0001308.
- [39] R. Blankenbecler and R. Sugar, *Phys. Rev.* **142**, 1051 (1966).
- [40] E. Epelbaum, W. Gloeckle, and U.-G. Meissner, *Nucl. Phys. A* **671**, 295 (2000), nucl-th/9910064.
- [41] M. Tanabashi et al. (Particle Data Group), *Phys. Rev. D* **98**, 030001 (2018).
- [42] Y.-H. Chen, D.-L. Yao, and H. Q. Zheng, *Phys. Rev. D* **87**, 054019 (2013), 1212.1893.
- [43] J. Gegelia and G. Japaridze, *Phys. Rev. D* **60**, 114038 (1999), hep-ph/9908377.
- [44] T. Fuchs, J. Gegelia, G. Japaridze, and S. Scherer, *Phys. Rev. D* **68**, 056005 (2003), hep-ph/0302117.
- [45] L. Geng, *Front. Phys. (Beijing)* **8**, 328 (2013), 1301.6815.
- [46] J.-X. Lu, L.-S. Geng, X.-L. Ren, and M.-L. Du, *Phys. Rev. D* **99**, 054024 (2019), 1812.03799.
- [47] V. Shtabovenko, R. Mertig, and F. Orellana, *Comput. Phys. Commun.* **256**, 107478 (2020), 2001.04407.
- [48] V. Shtabovenko, R. Mertig, and F. Orellana, *Comput. Phys. Commun.* **207**, 432 (2016), 1601.01167.
- [49] R. Mertig, M. Bohm, and A. Denner, *Comput. Phys. Commun.* **64**, 345 (1991).
- [50] A. van Hameren, C. G. Papadopoulos, and R. Pittau, *JHEP* **09**, 106 (2009), 0903.4665.
- [51] A. van Hameren, *Comput. Phys. Commun.* **182**, 2427 (2011), 1007.4716.
- [52] R. M. Woloshyn and A. D. Jackson, *Nucl. Phys. B* **64**, 269 (1973).
- [53] E. Epelbaum, W. Gloeckle, and U.-G. Meissner, *Eur. Phys. J. A* **19**, 401 (2004), nucl-th/0308010.
- [54] E. E. Salpeter and H. A. Bethe, *Phys. Rev.* **84**, 1232 (1951).
- [55] D. R. Entem and R. Machleidt, *Phys. Lett. B* **524**, 93 (2002), nucl-th/0108057.
- [56] E. Epelbaum, W. Gloeckle, and U.-G. Meissner, *Nucl. Phys. A* **747**, 362 (2005), nucl-th/0405048.
- [57] H. P. Stapp, T. J. Ypsilantis, and N. Metropolis, *Phys. Rev.* **105**, 302 (1957).
- [58] E. Epelbaum, W. Gloeckle, and U.-G. Meissner, *Eur. Phys. J. A* **19**, 125 (2004), nucl-th/0304037.
- [59] E. Epelbaum, H. Krebs, and U. G. Meißner, *Eur. Phys. J. A* **51**, 53 (2015), 1412.0142.
- [60] V. G. J. Stoks, R. A. M. Klomp, M. C. M. Rentmeester, and J. J. de Swart, *Phys. Rev. C* **48**, 792 (1993).
- [61] N. Kaiser, R. Brockmann, and W. Weise, *Nucl. Phys. A* **625**, 758 (1997), nucl-th/9706045.
- [62] D. R. Entem and R. Machleidt, *Phys. Rev. C* **66**, 014002 (2002), nucl-th/0202039.
- [63] D. R. Entem and R. Machleidt, *Phys. Rev. C* **68**, 041001 (2003), nucl-th/0304018.